Notice: This manuscript has been authored by UT-Battelle, LLC under Contract No. DE-AC05-00OR22725 with the U.S. Department of Energy. The United States Government retains and the publisher, by accepting the article for publication, acknowledges that the United States Government retains a non-exclusive, paid-up, irrevocable, world-wide license to publish or reproduce the published form of this manuscript, or allow others to do so, for United States Government purposes. The Department of Energy will provide public access to these results of federally sponsored research in accordance with the DOE Public Access Plan (http://energy.gov/downloads/doe-public-access-plan).

Magnetic structure and phase stability of the van der Waals bonded ferromagnet $Fe_{3-x}GeTe_2$

Andrew F. May,[1,*] Stuart Calder,[2] Claudia Cantoni,[1] Huibo Cao,[2] and Michael A. McGuire[1]

[1] *Materials Science and Technology Division, Oak Ridge National Laboratory, Oak Ridge, TN 37831*
[2] *Quantum Condensed Matter Division, Oak Ridge National Laboratory, Oak Ridge, TN 37831*

(Dated: December 16, 2015)

The magnetic structure and phase diagram of the layered ferromagnetic compound Fe_3GeTe_2 has been investigated by a combination of synthesis, x-ray and neutron diffraction, high resolution microscopy, and magnetization measurements. Single crystals were synthesized by self-flux reactions, and single crystal neutron diffraction finds ferromagnetic order with moments of $1.11(5)\mu_B$/Fe aligned along the *c*-axis at 4 K. These flux-grown crystals have a lower Curie temperature $T_C \approx 150$ K compared to crystals previously grown by vapor transport (T_C=220 K). The difference is a reduced Fe content in the flux grown crystals, as illustrated by the behavior observed in a series of polycrystalline samples. As Fe-content decreases, so does the Curie temperature, magnetic anisotropy, and net magnetization. In addition, Hall effect and thermoelectric measurements on flux-grown crystals suggest multiple carrier types contribute to electrical transport in $Fe_{3-x}GeTe_2$ and structurally-similar $Ni_{3-x}GeTe_2$.

I. INTRODUCTION

The extensive research on graphene and ultra-thin transition metal dichalcogenides (TMD) is naturally progressing into studies of van der Waals (VDW) bonded heterostructures and application-oriented configurations.[1–3] VDW heterostructures are produced from layer-by-layer stacking of monolayer (or few-layer) materials, which can be obtained from exfoliation of bulk sources.[4] These engineered structures will inevitably lead to unique properties and potentially new technologies, in part due to the ability to combine materials with complementary functionalities. This was recently demonstrated with the realization of highly-efficient, picosecond photoresponse in a heterostructure of graphene (fast response) and WSe_2 (high efficiency).[5] The construction of VDW heterostructures using topological insulators (TI) will certainly provide ample phase space for exploring novel states of matter and theoretical predictions. Currently, there is interest in controlling the dispersion and carrier type of the Dirac surface states of a TI using van der Waals heterostructures that allow separate tuning of bulk and surface states.[6]

VDW-bonded ferromagnets are of interest as building blocks for heterostructures designed for use in spin-based information technologies, either for the direct exploitation of their magnetic properties or via magnetic proximity effects. The latter permits the use of nominally non-magnetic materials in spintronics, and is being pursued using EuO/graphene heterostructures.[7,8] Similarly, skyrmions are of interest from a fundamental perspective and for their ability to potentially enable low-power spintronics, and these spin states are stabilized by a reduction from three to two dimensions and by the presence of Rashba spin-orbit coupling.[9,10] In general, spin-orbit coupling within heterostructures should yield interesting spin structures and magnetoelectric transport.

Of the 'next-generation' VDW materials, CrI_3 and $CrSiTe_3$-type compounds have recently been identified as promising systems with the potential for long-range magnetism in monolayers.[11–15] These materials are ferromagnetic at approximately 61 K and 33 K, respectively,[14,16] which is somewhat low for spintronic applications. Interestingly, magnetic odering temperatures have been predicted to increase when monolayers are constructed,[12] and initial experimental results seem to confirm this behavior in $CrSiTe_3$.[17] Considering this, the VDW-bonded compound Fe_3GeTe_2 may be of particular interest because the bulk is ferromagnetic near 230 K.[18]

Fe_3GeTe_2 contains Fe_3Ge slabs separated by VDW-bonded Te layers, as shown in Fig. 1(a). The Fe_3Ge slabs contain Fe(1)-Fe(1) pairs across a hexagonal network built by Fe(2)-Ge, and this is structurally similar to the more three-dimensional $Fe_{2-x}Ge$ compounds.[19] Fe_3GeTe_2 is an itinerant ferromagnet, with Curie temperatures of 220 and 230 K reported, and an estimated spontaneous magnetization of $1.6\mu_B$/Fe at 0 K.[18,20] Previous anisotropic magnetization measurements on crystals grown using chemical vapor transport suggested that the *c*-axis is the easy axis, and an anisotropy field of at least 5 T was demonstrated at 10 K.[20] The Fe(2) position was reported to have a small concentration of vacancies (17%), but chemical characterization suggested the composition is Fe_3GeTe_2.[18] Interestingly, Fe vacancies in $Fe_{2-x}Ge$ are also concentrated on the chemically similar Fe(2) position and a wide, complex phase-width is observed.[19] A modest phase-width is thus expected in Fe_3GeTe_2 based on the published crystallographic data, its intermetallic nature, and structural similarities with $Fe_{2-x}Ge$ compounds. Upon completion of this work, the existence of a phase-width was independently confirmed, though the influence on the structure and magnetic properties was not reported.[21]

We report the growth of single crystals via a molten

flux technique, together with a study of polycrystalline samples that confirms a phase width and corresponding response in the magnetic properties. We find that the lattice parameters, Curie temperature and saturation magnetization vary smoothly with Fe concentration, though the a and c lattice parameters trend oppositely. Reduced Fe content in the flux grown crystals is found to be responsible for their lower T_C when compared to prior reports. Additionally, we find that $Fe_{3-x}GeTe_2$ itinerant ferromagnets possess multi-carrier electronic transport.

II. EXPERIMENTAL DETAILS

Single crystals were grown from Fe-Ge-Te 'self'-fluxes, and a melt composition of Fe_2GeTe_4 produced the largest crystals of those investigated. Crystals were also successfully grown from the compositions $FeGe_2Te_4$ and $FeGeTe_2$ using similar heating procedures, though these crystals were typically smaller and had slightly lower Curie temperatures. High purity elements from Alfa Aesar (Fe 99.98%, Ge 99.9999%, and Te 99.9999%) were combined in Al_2O_3 crucibles and sealed in evacuated quartz ampoules. A crucible filled with quartz wool was placed on top of the growth crucible to catch the excess flux during centrifugation. The melt was homogenized at 950°C for approximately 12 h, then cooled slowly to 675°C, at which temperature the ampoules were removed from the furnace and placed in a centrifuge to expel the excess flux. A variety of cooling rates were found to produce crystals, and in this paper we report data from crystals obtained after cooling at 1 and 3°/h (the properties were observed to be equivalent). We also synthesized crystals of Ni_3GeTe_2 to provide a non-magnetic reference material during our investigation of transport properties. Crystals of Ni_3GeTe_2 were grown from a melt of $NiGeTe_2$ cooled at 3°/h, with the flux removed at 660°C. The crystals of Ni_3GeTe_2 were generally smaller than those of Fe_3GeTe_2. Upon characterization, both were found to be transition metal deficient.

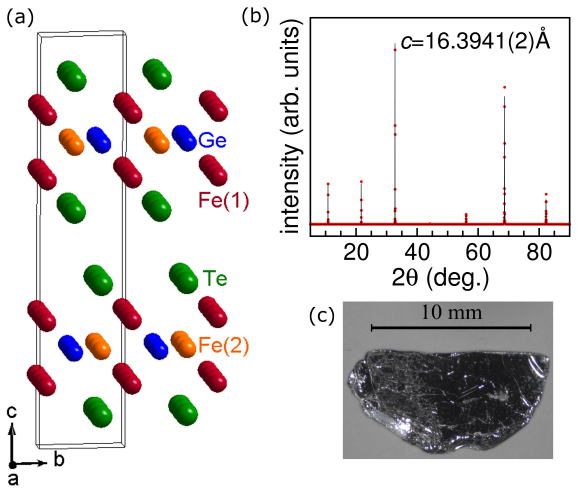

FIG. 1. (color online). (a) Image of crystal structure with atomic positions labeled; Fe(1)-Fe(1) bonds pierce the center of each hexagon formed by Fe(2)-Ge (space group $P6_3/mmc$ - no. 194). (b) X-ray diffraction data for an as-grown facet of Fe_3GeTe_2 showing the c-axis normal with exclusively 00l diffraction peaks observed; a Le Bail fit (solid line) yielded the c-axis lattice parameter shown in the image. (c) A picture of a large single crystal.

Polycrystalline samples with nominal Fe concentrations between $Fe_{3.10}GeTe_2$ and $Fe_{2.60}GeTe_2$ were prepared by grinding Fe powder, Ge powder, and Te shot in a He filled glove box. The mixture was transferred, under He, to a vacuum line where the quartz ampoule was sealed under vacuum. The samples were heated at 675°C for approximately 10 d. The as-reacted $Fe_{3-x}GeTe_2$ samples were found to be either slightly sintered and dull black for small x, or heavily sintered with visible grain growth/crystallization for large x. At this point, the samples were analyzed with x-ray diffraction and magnetization measurements. Small pellets were then fired briefly at 600°C to facilitate isothermal magnetization and energy dispersive spectroscopy (EDS) measurements. EDS measurements were performed using a Bruker Quantax 70 EDS system on a Hitachi TM-3000 microscope.

Crystals from the flux-grown reactions are much larger than those needed for single crystal x-ray diffraction. Due to the ease with which the crystals cleave and deform, the process of cutting or crushing the crystals induces significant damage. Therefore, a small crystal from the polycrystalline reaction with nominal composition $Fe_{2.75}GeTe_2$ was selected for single crystal x-ray diffraction. Data were collected at 173 K on a Bruker SMART APEX CCD, using Mo-$K\alpha$ radiation (λ = 0.71073 Å, graphite monochromator). For refinement of the crystal structure, absorption corrections were applied with SADABS and SHELXL-97 was used to refine the data, and the atomic coordinates were standardized with Structure Tidy within PLATON.[22–24] The refinement utilized 138 unique reflections from 1885 reflections and 12 refinement parameters. The Goodness of Fit was 1.303 while R_{int} = 0.0280. Powder x-ray diffraction data were collected using a PANalytical X'Pert Pro MPD with a Cu $K_{\alpha,1}$ (λ=1.5406 Å) incident beam monochromator, and Le Bail and Rietveld refinements were performed using FullProf.[25]

Magnetization measurements were performed in a Quantum Design Magnetic Property Measurement System, as well as with the AC Magnetic Susceptibility Option on a Quantum Design Physical Property Measurement System (PPMS). A PPMS was also used to measure the Seebeck coefficient, thermal conductivity and electrical resistivity using the Thermal Transport Option. For this measurement, gold-coated copper leads were attached to the crystals using H20E Epo-Tek silver epoxy. Hall effect measurements and magnetoresistance measurements were performed using a standard four-point configuration with Pt wires attached via sil-

ver paint (DuPont 4929N). The Hall resistance ρ_H was obtained via the odd-in-$\boldsymbol{H}$ part of the transverse resistance $\rho_H = (\rho_{xy}[\boldsymbol{H}] - \rho_{xy}[\boldsymbol{-H}])/2$ with maximum magnetic fields of magnitude H=80 kOe applied along the c-axis. Magnetoresistance was obtained from the even-in-$\boldsymbol{H}$ portion of the longitudinal resistance with fields applied along the c-axis. At 2 K and 80 kOe, the magnetoresistance was less than 2% and we have excluded the data from the manuscript.

To probe the microscopic crystal and magnetic structure, we performed single crystal neutron diffraction on the Four-Circle Diffractometer (HB-3A) at the High Flux Isotope Reactor (HFIR), ORNL. A single crystal of approximate dimensions 4 mm × 4 mm was mounted on an Al rod inside a CCR. Using an incident wavelength of 1.003 Å (Si(331) monochromator), measurements were performed between 4 K and room temperature. A large number of reflections were collected at 220 K and 4 K to determine the nuclear and magnetic structures, respectively. Neutron powder diffraction was performed on the HB-2A Neutron Powder Diffractometer at HFIR, ORNL. A wavelength of 2.41 Å was used in all measurements, and this was selected with a Ge(113) monochromator; the samples were placed in Al cans. All neutron diffraction data were refined using the program FullProf.[25]

High resolution scanning transmission electron microscopy (STEM) was performed using a Nion UltraSTEM200 microscope operating at 200 keV, equipped with a Gatan Enfinium spectrometer for the in situ collection of electron energy loss spectra (EELS). Samples were examined in both plan view and cross-sectional orientations. Samples were prepared by a combination of polishing and Ar^+ ion milling using a voltage of 2 keV. Contact with moisture was avoided during sample preparation.

III. RESULTS AND DISCUSSION

The single crystals obtained from self-flux growths are thin plates with dimensions reaching greater than 1 cm (see Fig. 1). X-ray diffraction data collected from the surface of as-grown facets confirm the expected orientation with [00l] normal to the facet, as shown in Fig. 1. A Le Bail fit to the diffraction data in Fig. 1 yielded c=16.3941(2)Å. Rietveld refinement of data collected on ground crystals resulted in a=3.9536(7)Å and c=16.396(2)Å. These values differ sharply from those in the literature, where a=3.9910(10)Å and c=16.336(3)Å were reported from room temperature single crystal x-ray diffraction.[18]

Ni_3GeTe_2 crystals were grown from a self-flux to provide a non-magnetic reference material during the characterization of physical properties. The lattice parameters obtained for our Ni_3GeTe_2 crystals also differ from those in the literature, with refinement of powder diffraction data yielding a=3.8373(2)Å and c=16.048(2)Å. This compares to a=3.9110(10)Å and c=16.022(3)Å

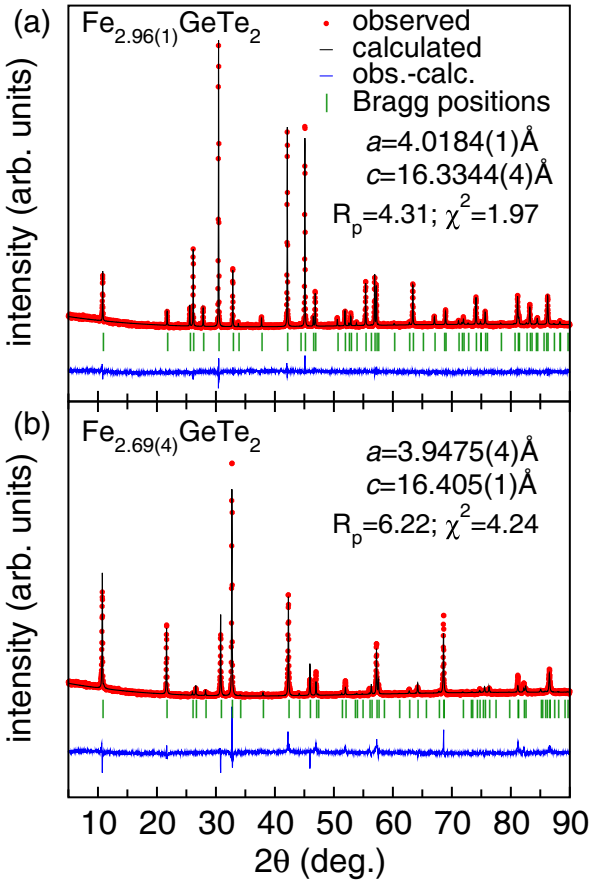

FIG. 2. (color online). Powder x-ray diffraction data for two polycrystalline samples with refined lattice parameters and compositions provided.

previously reported for crystals with a composition of $Ni_{2.95}GeTe_2$ obtained from refinement of single crystal x-ray diffraction data.[18] Thus, for both Fe_3GeTe_2 and Ni_3GeTe_2 grown from a self-flux, the a lattice parameter is smaller and the c lattice parameter is slightly larger than the literature reports for crystals obtained from nominal 3-1-2 compositions (formed via solid state reactions).

In addition to having different lattice parameters than those in the literature, the flux-grown Fe_3GeTe_2 crystals have lower Curie temperatures than those previously reported for Fe_3GeTe_2. The crystals were grown from self-fluxes, which minimize the chance for extrinsic doping. We thus speculated that Fe_3GeTe_2 contains a non-trivial phase width that influences structure and physical properties. Our EDS results suggest Fe and Ge deficiencies may exist, with a composition of $Fe_{2.91(3)}Ge_{0.95(4)}Te_{2.00(4)}$ obtained. For the Ni-based analogue, EDS yielded $Ni_{2.40(4)}Ge_{1.01(3)}Te_{2.00(3)}$ for crystals grown from $NiGeTe_2$.

To investigate the phase width of $Fe_{3-x}GeTe_2$, polycrystalline samples were produced via solid-state reactions with nominal compositions $Fe_{3-x}GeTe_2$ with $-0.1 \leq x \leq 0.4$. These materials were characterized

using powder x-ray diffraction, EDS, and magnetization measurements. We begin by presenting the results of our crystallographic studies, and then return to the magnetic properties and detailed characterization of our single crystals. When necessary for unit conversion, we have utilized compositions obtained by Rietveld refinement. When discussing single crystals, we present data for crystals grown from Fe_2GeTe_4 melts, and refer to these by the composition obtained from refinement of single crystal neutron diffraction data, $Fe_{2.76}Ge_{0.94}Te_2$.

A. Structure and Composition

All polycrystalline samples were found to be phase pure within the limits of our powder x-ray diffractometer, with the exception being a sample of nominal composition $Fe_{2.60}GeTe_2$. This sample contained GeTe and $FeTe_2$ impurities, and data for this sample have been excluded from the manuscript. Our results thus suggest the Fe-deficient phase boundary is likely reached near $Fe_{2.7}GeTe_2$. We have not investigated the phase width with regard to Te or Ge.

The sample of nominal composition $Fe_{3.10}GeTe_2$ did not possess any obvious impurities by x-ray diffraction. The refined composition for this sample is $Fe_{2.97(2)}GeTe_2$, while large-area (300 μm diameter) EDS scans yielded $Fe_{3.07(2)}Ge_{0.92(2)}Te_{2.00(2)}$. The EDS results are likely influenced by minor secondary phases that are not easily detected by x-ray diffraction. An Fe-rich impurity was observed in back scattered electron images, and we were not able to isolate large grains of the main phase for EDS due to resolution limits. Therefore, we focus on compositions obtained from Rietveld refinements of the powder diffraction data. In the structurally-similar Ni_3GeTe_2 compound, occupation of an interlayer Ni(3) position at (0,0,0) was detected by single crystal x-ray diffraction, though occupation of this site was not observed in Fe_3GeTe_2.[18] We performed refinements including the hypothetical Fe(3), and the results suggest that an occupation of 3(1)% may exist for the nominal $Fe_{3.10}GeTe_2$. This seems reasonable, but the result is dependent on the range of data analyzed (in part due to a connection to the refinement of sample texture). Based on our single crystal diffraction and electron microscopy, discussed below, we feel confident that there is not any significant occupation of this interlayer site in the nominally Fe-deficient samples (at least for $x \approx 0.25$). We therefore utilized the published crystal structure, with two Fe positions, to refine our diffraction data and report compositions based on this refinement.

Figure 2 presents powder x-ray diffraction data and Rietveld refinements for samples of nominal composition $Fe_{3.00}GeTe_2$ and $Fe_{2.75}GeTe_2$, which refined to the compositions $Fe_{2.96(1)}GeTe_2$ and $Fe_{2.69(4)}GeTe_2$, respectively. The lattice parameters obtained from refinement of the data in Fig. 2 confirm that the Fe-deficient sample has smaller a and larger c than the Fe-rich sample. This

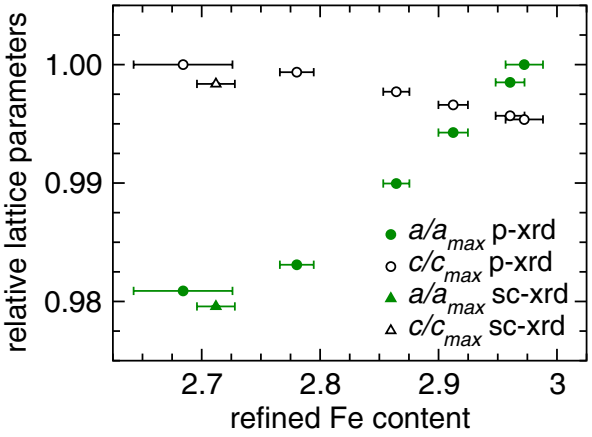

FIG. 3. Normalized lattice parameters as a function of refined Fe content for $Fe_{3-x}GeTe_2$ samples (powder x-ray diffraction 'p-xrd' at room temperature), including results obtained from single crystal x-ray ('sc-xrd') diffraction data collected at 173 K; $a_{max} = 4.0244(1)$ Åand $c_{max} = 16.405(1)$ Å. Vertical error bars are smaller than the size of the data markers.

trend is shown in Fig. 3 for all polycrystalline samples, where the normalized lattice parameters are plotted as a function of Fe content. Data obtained from single-crystal x-ray diffraction (sc-xrd) are also included to confirm this behavior; note that the sc-xrd data were collected at 173 K where slightly smaller lattice parameters are expected. The increase in a with increasing Fe may be expected, with the lattice expanding as Fe(2) vacancies are filled. Indeed, a similar trend in a occurs for $Fe_{2-x}Ge$ in the range $0.15 < x < 0.7$, though c was found to increase with increasing Fe content in this more 3D compound.[19]

Given the layered structure, we expect the greatest influence of the increased occupation of Fe(2) to be observed within the (Fe_3Ge) planes. Indeed, the relative expansion of a is greater than the relative contraction of c (see Fig. 3). We therefore expect the changes in c to be driven by the changes in a. That is, the decrease in c is due to an expansion of the basal plane that allows Te atoms to get closer to the Fe_3Ge layer, while increased occupation of Fe(2) also leads to greater Fe(2)-Te bonding. Consistent with this, Fe(2)-Te bond distances are smallest in the Fe-rich samples, as are Fe(1)-Fe(1) bond distances. As a result of Te being pulled towards the Fe_3Ge layers, the structure collapses along c to maintain the van der Waals bonds (the length of which increases with increasing Fe). If the hypothetical Fe(3) becomes occupied at high Fe concentrations, its presence could lead to increased bonding that would also reduce c. However, refinements with Fe(3) reveal a larger Fe(3)-Te bond distance for higher Fe contents, suggesting that Fe(3) does not play a role in the contraction of c.

We note that the occupancy of Fe(2) is correlated to the refinement of texture (preferred orientation) in the powder diffraction data. In these samples, the texture physically increases with decreasing Fe content. This trend can be observed visually, with the Fe-deficient sam-

ples demonstrating more grain growth during the reaction. Not refining the texture results in much larger residuals, and thus the preferred orientation was refined for all samples and care was taken to minimize the texture during sample preparation. The main result is not strongly influenced by this, though, and the nominal composition clearly influences the amount of Fe in the final specimen and the trends are consistent. Also, to simplify the refinement, we did not allow Ge content to vary and fixed an overall displacement parameter.

TABLE I. Selected data from refinements of single crystal x-ray diffraction collected on a crystal from a reaction of nominal composition $Fe_{2.75}GeTe_2$. Atomic coordinates are Fe(1): 0,0,z; Fe(2): $\frac{1}{3},\frac{2}{3},\frac{1}{4}$; Te: $\frac{1}{3},\frac{2}{3},z$; Ge: $\frac{1}{3},\frac{2}{3},\frac{3}{4}$.

a (Å)	3.9421(9)
c (Å)	16.378(5)
R_1 (all data)	0.0461
wR_2 (all data)	0.1019
Goodness of fit	1.306
Fe(1) z coord.	0.1721(2)
Te z coord.	0.0900(1)

The potential existence of interlayer Fe is important beyond understanding the modifications to the lattice with changing Fe content. As shown below, the total Fe content clearly influences the magnetic properties and interlayer Fe could play a particularly important role in determining the saturation magnetization and coercive field. In regards to the chemistry and structure of these materials, the existence of interlayer Fe would imply a more three-dimensional material. As such, interlayer Fe would likely impede the production of thin-layers by cleaving bulk crystals. Similarly, if an amount of interlayer Fe can be controlled, it would likely influence the anisotropy of the electronic and magnetic properties. Interestingly, as discussed below, the samples with the highest Fe content have the largest anisotropy in the magnetic properties. While our powder diffraction results suggest Fe(3) is not occupied, we felt that additional investigation was warranted.

We investigated the issue of interlayer Fe with single crystal x-ray and neutron diffraction, and electron microscopy. The refinement results from the x-ray diffraction data are shown in Table I, and we clearly observe the partial occupation of Fe(2) with a refined composition $Fe_{2.71(2)}GeTe_2$ (recall this is for a crystal obtained from the $Fe_{2.75}GeTe_2$ polycrystalline reaction; Ge vacancies were not observed). Electron density was not detected at an interlayer Fe(3) position, consistent with earlier work for crystals selected from a polycrystalline sample of nominal composition Fe_3GeTe_2.[18] Our single crystal neutron diffraction on flux-grown crystals, discussed in more detail below, does not find any strong evidence for occupation of the Fe(3) position.

A large number of vacancies are refined on the Fe(2) position from both the neutron and x-ray single crystal diffraction data. When filled, these Fe(2) positions are bonded to three in-plane Ge atoms. As vacancies are introduced, Fe(2)-Ge bonding decreases (on average) and this results in a large in-plane displacement parameter for Ge, as shown in Table II. Consistent with this, we refine a larger concentration of vacancies on Fe(2) compared to Ref. 18, and our refined U_{11} for Ge is also larger than previously reported. However, the previous study did report a strong anisotropy for the displacement parameters of Ge, and a similar U_{33} to that shown in Table II was reported.[18] In the binary compound $Fe_{1.60}Ge_2$, it has been suggested that the Ge atoms actually move off of their site and the symmetry is potentially broken.[26]

TABLE II. Anisotropic displacement parameters for $Fe_{3-x}GeTe_2$ from refinements of single crystal x-ray diffraction data at T=173 K; note $U_{11} = U_{22} = 2U_{12}$.

species	U_{11} Å^2	U_{33} Å^2	U_{eq} Å^2	occupancy fractional
Fe(1)	0.0069(12)	0.014(2)	0.0091(10)	1
Fe(2)	0.0069(12)	0.014(2)	0.0091(10)	0.71(2)
Ge	0.044(2)	0.015(2)	0.034(1)	1
Te	0.0081(6)	0.0152(8)	0.0105(5)	1

The data in Table II correspond to refinement of single crystal x-ray diffraction data, where only Fe(2) was found to be partially occupied. We obtained a fractional occupation of 0.71(2) for Fe(2), and this was utilizing a constraint to maintain equal displacement parameters for Fe(1) and Fe(2). When refined separately, the displacement parameters of Fe(2) are observed to be rather small within the basal plane (U_{11}=0.004(2)). In this case, the refined occupancy of Fe(2)=0.69(2) is very similar to that obtained from the restrained fit.

We also performed high resolution scanning transmission microscopy (STEM) to investigate the local structure. For imaging, we used the high angle annular dark field detector (HAADF), which yields a contrast nearly proportional to Z^2 (Z = atomic number) and is therefore better suited for imaging vacancies and interstitials, and cations with different atomic numbers.

A representative cross-sectional image with the electron beam parallel to [130] is shown in Fig. 4(a), and plan view images with the electron beam parallel to [001] were also collected but are not shown. In general, the crystals looked to be of high quality, lacking obvious two or three dimensional defects. In the Z-contrast images, the van der Waals gaps between layers of Te atoms (brightest spots) can be easily identified and intensity is not observed between them, suggesting that interlayer Fe is not present in our crystals. In both cross-sectional and plan view images, we observe a variation in the intensity of the atomic columns containing Fe(2) and Ge, which is consistent with the presence of Fe vacancies. The intensity profiles in Fig. 4(b) reveal these variations, with the Fe(2)-Ge columns displaying a clear disruption of the pattern expected for the case of fully occupied Fe(2) sites. Due to the difference in Z between Fe (Z=26) and Ge (Z=32), a fully occupied structure would display higher-intensity

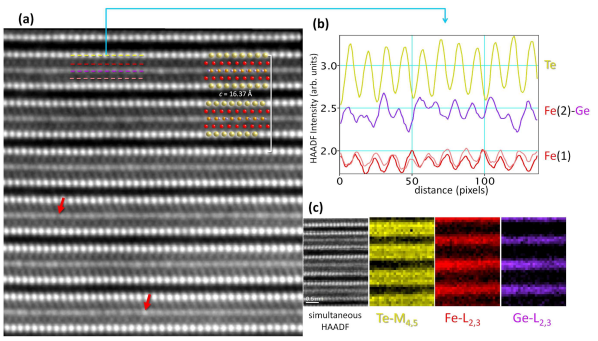

FIG. 4. (color online) HAADF STEM image showing Z-contrast. The heaviest columns (Te) show up as the brightest spots and Fe columns show up with the dimmest contrast. Van der Waals gaps are clearly visible as black stripes. The inset shows an overlay of the lattice projection along [130]. (b) Profiles of the intensity along the dashed lines shown in (a) indicating significant disorder in the Fe(2)-Ge plane. (c) EELS integrated intensity maps showing the chemical signature of the alternating Te, Fe, and Fe-Ge planes.

peaks adjacent to lower-intensity peaks in a high-low-high sequence when viewed down [130]. The red arrows in the image highlight Fe and Ge columns with markedly lower or higher intensity compared to the average. Based on the images, we cannot exclude the possibility of Ge-Fe antisite defects or Ge vacancies in the Fe(2)-Ge planes. Due to the low vacancy concentration and the more delocalized nature of the EELS signal as compared to the HAADF signal, vacancies are not resolved in the EELS compositional maps shown in Fig. 4(c), which show a uniform distribution for the integrated intensities of the Te-$M_{4,5}$, Fe-$L_{2,3}$ and Ge-$L_{2,3}$ edges.

The images were observed to change upon continued exposure to the electron beam. A movement of atoms and vacancies could be observed, with atoms eventually occupying the interlayer region and vacancies appearing to occupy sites besides Fe(2). In order to avoid beam-induced hopping and preserve observation of the intrinsic structure, images were collected rapidly on unirradiated regions by summing 20 frames, each one acquired within 1 s. EEL spectrum images were acquired using a spacing of 0.87 Å and a dwell time of 0.2 s. Beam-induced structural effects were also noted for Ni_3GeTe_2 in Ref. 18.

EELS was utilized to look for differences in the oxidation state of the two Fe sites. The ratio of the Fe $L_{3,2}$ peaks gives an indication regarding the oxidation state, though this can vary with details of the bonding environment. We find an $L_{3,2}$ ratio that varies slightly between the Fe(1) and Fe(2) positions, which may suggest the Fe atoms are in slightly different oxidations states or carry a different moment.

The lack of evidence for occupation of Fe(3) in the STEM and diffraction studies may be due to the low-occupation of this position, which is likely to be further

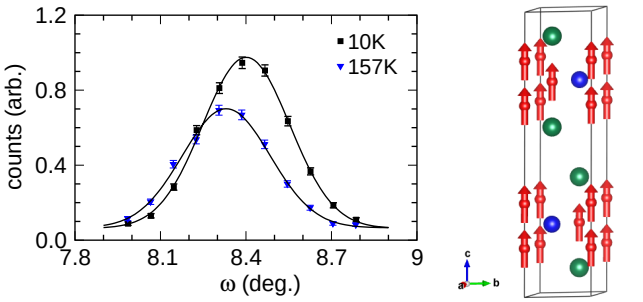

FIG. 5. (color online). Rocking curves of the 010 reflection from single crystal neutron diffraction on $Fe_{2.76}Ge_{0.94}Te_2$ at 10 K and 157 K. The solid lines are Gaussian fits to the peaks. The image on the right shows the magnetic structure obtained by refinement of neutron diffraction data collected at 4 K (Fe = red, Te = green, Ge = blue).

reduced with the overall decrease of Fe content in our crystals due to the flux growth. Examination of Fe-rich crystals will offer the best chance for identifying interlayer Fe, if it exists, though even then the concentration will likely be very small and observation will be challenging. Even at such low concentrations, though, the presence of interlayer Fe could strongly influence the physical properties.

B. Neutron Diffraction

Single crystal neutron diffraction was performed on a crystal obtained from the Fe_2GeTe_4 flux. This flux composition was found to produce the largest crystals, and thus it was investigated in the most detail (including magnetization and transport measurements below). The crystal structure was refined using data collected at 220 K, and the magnetic structure was obtained from data collected at 4 K. As discussed below, powder neutron diffraction measurements were also performed to verify the magnetic structure and investigate variations in the Fe moment(s) as a function of composition.

Figure 5 shows representative rocking curves obtained during the single crystal neutron diffraction data collection. As shown, there is strong temperature dependence that indicates the presence of magnetic order below 157 K. The nuclear refinement is consistent with the single crystal and powder x-ray diffraction data. We refine vacancies at the Fe(2) and Ge sites, and do not observe strong evidence for Fe substituting for Ge. Consistent with the above discussion, we do not detect any Fe between the Te-Te layers. The refined composition is $Fe_{2.76(4)}Ge_{0.94(4)}Te_2$ with R_F=4.11 and χ^2=0.423. The site occupancies were fixed to these values for the lower temperature refinements.

An ordered moment along $\boldsymbol{c}$ of 1.11(5)μ_B/Fe is obtained from refinement of the single crystal data at 4 K, and a schematic of the magnetic structure is shown in Fig. 5. Our refinement does not indicate any signifi-

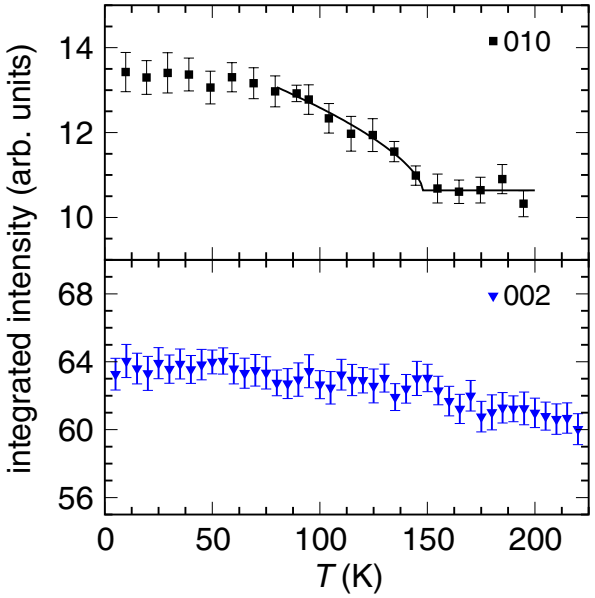

FIG. 6. (color online). Integrated intensities of Bragg peaks from single crystal neutron diffraction on $Fe_{2.76}Ge_{0.94}Te_2$. The increase in intensity for the 010 peak below T_C originates from the magnetic order along c, whereas the intensity of the 002 peak does not change significantly with temperature.

cant difference in the moments on the two Fe positions for the Fe-deficient crystal. If we allow both moments to refine separately, we obtain $1.07(11)\mu_B$/Fe(1) and $0.9(5)\mu_B$/Fe(2). We note that the errors on the moment values increase appreciably when both are allowed to refine separately, and this gives values consistent with that for fixed Fe(1) and Fe(2). Thus, within the limits of this data, we have no reason to suspect that the different sites carry significantly different moments at this Fe concentration. Very recently, based on powder neutron diffraction data from $Fe_{2.9}GeTe_2$, the ratio of moments between Fe(1) and Fe(2) was found to be 1.25 at 1.5 K.[21] For comparison, in $Fe_{1.76}Ge$ the ordered moments lie in the ab-plane, and an average moment of $1.56\pm0.2\mu_B$/Fe was reported based on neutron diffraction.[27] There have been contradictory reports regarding a variation of the moments between the two Fe sites in $Fe_{2-x}Ge$.[27–29] The more recent Mössbauer results have suggested that a larger moment resides on the Fe(2) site, and perhaps similar experiments on Fe_3GeTe_2 may provide additional insight into the roles of the different Fe environments. The difference in the easy axis between Fe_3GeTe_2 and $Fe_{1.67}Ge$ is most likely caused by the increased chemical anisotropy associated with the inclusion of the Te-Te layer into the Fe_3GeTe_2 structure.

We confirmed the ferromagnetic ordering temperature and orientation of the moments by tracking the 010 and 002 Bragg peaks, as shown in Fig. 6. The power law fit between 80 K and 180 K in Fig. 6 yields $T_C = 148(3)$ K, which is consistent with the bulk magnetization measurements. The intensity of the 010 peak increases when the moments lie perpendicular to the 010 scattering vector. Therefore, the increase in intensity below ≈ 150 K shown in Fig. 6(a) demonstrates that the moments do not lie along the b-axis, and when combined with the temperature-independent behavior of 002 intensity we verify that the moments lie along $\boldsymbol{c}$. This shows that there is not any significant spin canting or reorientation as temperature decreases, which is also confirmed with the powder neutron diffraction measurements. In addition, we did not observe any significant change in the nuclear structure across the magnetic transition.

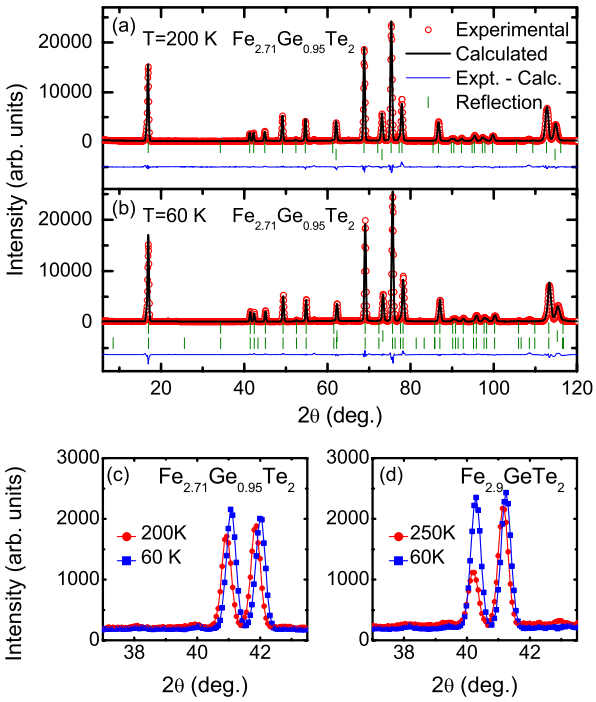

FIG. 7. (color online). Neutron powder diffraction at (a) 200 K and (b) 60 K with refinements included and samples labeled by the refined compositions. The reflections from top to bottom correspond to the structural, aluminum can and magnetic reflections. The most intense magnetic signal was observed in the region shown in figures (c) and (d). Note the much increased magnetic intensity in the $Fe_{2.9}GeTe_2$ sample compared to the more Fe-deficient $Fe_{2.71}GeTe_2$.

During the single crystal neutron diffraction measurements, we scanned along H and L and found no additional non-integer (H,K,L) intensity through the magnetic transition of 150 K. Additionally, in the neutron powder diffraction data shown in Fig. 7, there is no evidence of scattering at non-integer (HKL) positions in going from above the Curie temperature T_C to below T_C. This strongly suggests that there is no deviation from the observed ferromagnetic structure for both Fe-rich and Fe-deficient samples. We did notice some diffuse scattering beneath the Bragg peaks in our single crystal neutron diffraction, and this scattering was persistent at temperatures well above the magnetic ordering. As such, this is likely related to crystalline defects and requires further

TABLE III. Summary of refinements of powder neutron diffraction data. Refined compositions are the result of refining the occupation of the Fe(2) position. Refined moments are aligned along the c-axis.

Nominal Composition	T (K)	Refined Fe	a (Å)	c (Å)	moment Fe(1) (μ_B)	moment Fe(2) (μ_B)	R_P
Fe_3GeTe_2	250 K	2.904(8)	4.01749(8)	16.33990(8)	-	-	3.02
Fe_3GeTe_2	60 K	2.904(8)	4.00938(3)	16.2850(2)	2.18(10)	1.54(10)	3.41
$Fe_{2.75}GeTe_2$	200 K	2.71(3)	3.95001(7)	16.4019(4)	-	-	3.42
$Fe_{2.75}GeTe_2$	60 K	2.71(3)	3.93628(4)	16.3535(3)	1.4(1)	1.4(1)	5.25

investigation (note that stacking faults were not observed in our STEM).

Neutron powder diffraction was performed on polycrystalline samples of nominal compositions Fe_3GeTe_2 and $Fe_{2.75}GeTe_2$ (see Fig. 7 where refined compositions are utilized). In both cases, no deviation from the magnetic structure obtained from single crystal neutron diffraction was observed, indicting similar ferromagnetism regardless of Fe concentration. The refinement results are summarized in Table III. The Fe-rich sample, with a refined composition of $Fe_{2.90}GeTe_2$, was found to have a stronger magnetic contribution to the Bragg peaks and the refinement yielded a larger ordered moment on Fe(1) than on Fe(2) (the raw data for this sample are shown in the Supplemental Materials). Fixing the moments to be the same on the Fe(1) and Fe(2) sites did not provide suitable fits to the data for this sample. This result is consistent with a recent publication containing neutron powder diffraction on a sample of $Fe_{2.90}GeTe_2$.[21] The behavior is different in the Fe-deficient sample, which has a refined composition of $Fe_{2.71}Ge_{0.95}Te_2$. In this sample, the magnetic contribution to the diffraction peaks is smaller and appears similar for both Fe(1) and Fe(2). The refined moment is slightly larger than that obtained on the single crystal (similar composition), but the trend for similar moments on the Fe(1) and Fe(2) sites is consistent. This suggests that vacancies on the Fe(2) site suppress the magnetism on both Fe sites. This could be related to the changes in structural parameters, though disorder and/or dilution effects may also be dominant.

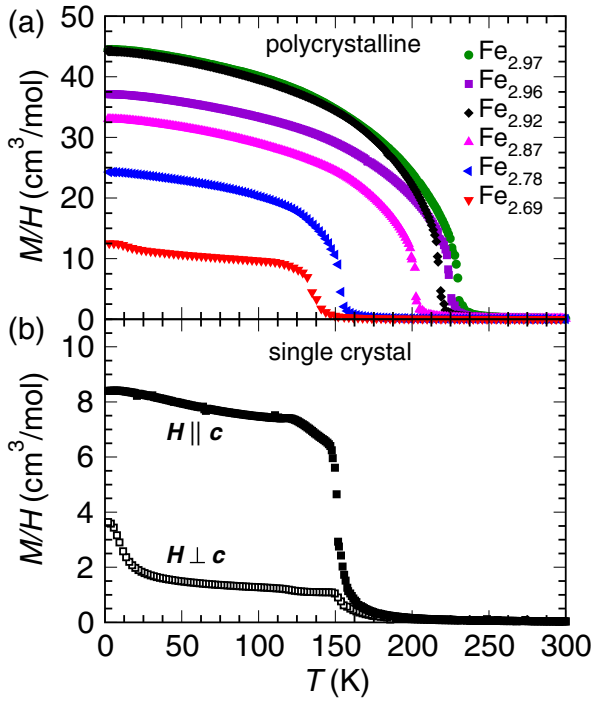

FIG. 8. (color online) (a) Temperature dependence of the magnetization M divided by applied field H for polycrystalline $Fe_{3-x}GeTe_2$ materials with various Fe concentrations as indicated by the refined Fe content in the legend, and (b) anisotropic magnetization of flux-grown $Fe_{2.76}Ge_{0.94}Te_2$. All data were collected upon cooling in an applied field of H=100 Oe.

C. Magnetization

Magnetization measurements were performed on the polycrystalline materials to determine their Curie temperatures and correlate this with structure and composition. Results of the temperature-dependent magnetization M measurements are shown in Fig. 8(a), where refined Fe contents are used in the legend. We have used Gaussian-CGS units for the magnetization results.

The data in Fig. 8(a) demonstrate that the Curie temperature decreases with decreasing Fe content. The reduced T_C with increasing vacancies on the Fe(2) site may be caused by a disruption of the magnetic exchange with increasing disorder and magnetic dilution via vacancies. There may also be a structural component, as we observe that the reduced T_C correlates with the expansion of c, an increase in Fe(1)-Fe(1) bond distance, and decrease in Fe(1)-Fe(2) bond distances. A similar reduction in T_C is observed for $Fe_{2-x}Ge$ materials as x increases, though, where a more typical decrease in the lattice parameters is observed with increasing x.[19] Investigating the pressure-dependence of T_C or the anisotropy of the magnetic excitation spectra may provide further insight, as would theoretical calculations into the dependence of T_C on c.

Anisotropic magnetization data for single crystalline $Fe_{3-x}GeTe_2$ are shown in Fig. 8(b). These data demonstrate that the easy axis for magnetization is along the crystallographic c-axis, which is consistent with our neutron diffraction and Ref. 20. The shape of $M(T)$ evolves with decreasing Fe content. In the Fe-rich samples, $M(T)$ increases smoothly while cooling. In contrast, for the most Fe-deficient sample, $M(T)$ has a kink-containing

shape near T_C and essentially plateaus slightly below T_C. The $M(T)$ data reported on the vapor transport crystals, with $T_C \approx 220\,K$, has a temperature dependence similar to that shown in Fig. 8(b). Therefore, the non-power law behavior observed near T_C in the single crystals may be linked to domain wall formation and movement. It is certainly possible that different growth conditions produce different Fe(2)/Fe(3) contents, which could also modify the properties independently. We also confirmed that $Ni_{3-x}GeTe_2$ appears to be a Pauli paramagnet.

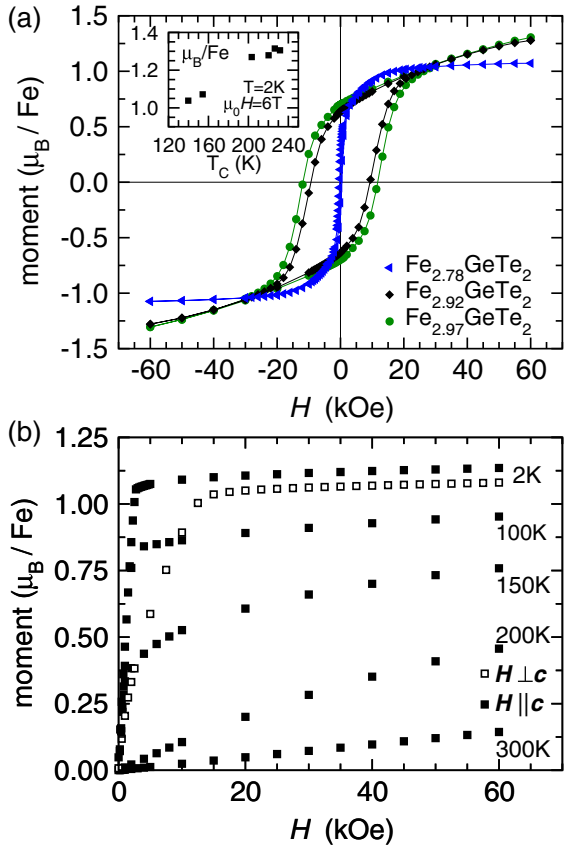

FIG. 9. (color online). (a) Magnetization loops at 2 K for three compositions of polycrystalline $Fe_{3-x}GeTe_2$ (refined values provided), and the inset shows the magnetization at 2 K and 60 kOe for polycrystalline samples. (b) Magnetization versus applied field for single crystalline $Fe_{2.76}Ge_{0.94}Te_2$ at various temperatures, with the anisotropy demonstrated at 2 K.

Isothermal magnetization data are shown in Fig. 9. In panel (a), data for three polycrystalline samples are shown while panel (b) contains data for an oriented single crystal. The isothermal magnetization measurements for polycrystalline samples reveal some interesting trends with composition. It is clear that the Fe-deficient samples have a much lower remanent magnetization and very little coercivity. Also, the moment essentially saturates at high fields for the Fe-deficient samples while a linear rise with field is observed for the Fe-rich samples. The linear increase at higher fields for $Fe_{2.97}GeTe_2$ may be related

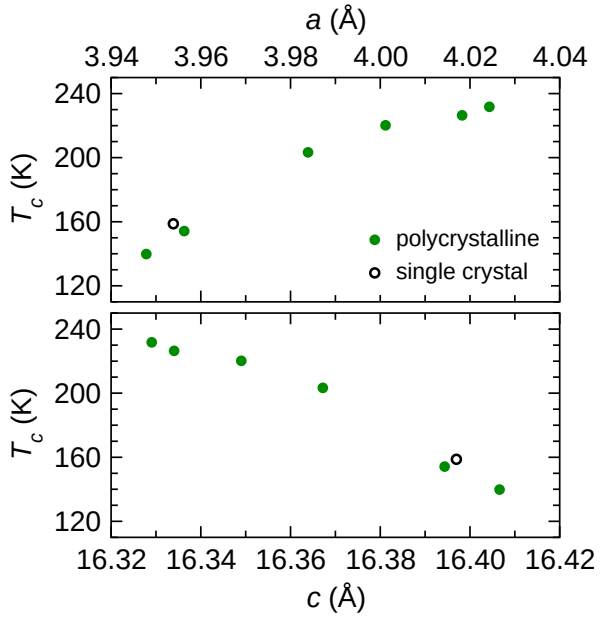

FIG. 10. (color online). Curie temperature as a function of lattice parameters for $Fe_{3-x}GeTe_2$.

to an increased anisotropy field at higher Fe content. Our low-Fe content crystals have an estimated anisotropy field of 15 kOe (or 1.5 T), as shown in Fig. 9(b). An anisotropy field of ≈5 T was observed at 10 K for crystals grown by vapor transport,[20] and the reported $T_C \approx 220$ K suggests a large Fe content in those crystals. The linear rise at large fields may be also be from some paramagnetic ions, such as an impurity or interlayer Fe. We note that our $Fe_{2.76}Ge_{0.94}Te_2$ crystals did not reveal any unexpected behavior when measured to 120 kOe.

The 'saturation magnetization' of all polycrystalline $Fe_{3-x}GeTe_2$ samples is shown as an inset in Fig. 9(a) and values are listed in the summary of samples provided as Table IV. The saturation magnetization is taken as the value of the magnetization (in μ_B/Fe) obtained at 2 K and 60 kOe (refined compositions are used for unit conversion). This does not represent a true saturation magnetization for all samples due to the linear increase in M at large H. We clearly see that higher T_C (higher Fe content) correlates with larger induced moments for a given T at large applied fields, consistent with our powder neutron diffraction results. T_C was defined using the intercept of the steepest tangent. The effective moments calculated from the susceptibility (χ) between 250 and 360 K were found to vary between 3.9(2) and 4.9(1)μ_B/Fe, with higher T_C generally corresponding to larger effective moments. We used a standard Curie-Weiss law ($\chi = C/(T - T_{CW})$) and fit data collected on cooling in an applied field of 1 kOe. Curie-Weiss temperatures T_{CW} obtained from these fits agreed well with the Curie temperatures obtained from measurements at lower fields.

We calculated the Rhodes-Wohlfarth ratio (RWR)

TABLE IV. Summary of samples and magnetic properties for polycrystalline $Fe_{3-x}GeTe_2$. Rietveld compositions originate in refinement of powder diffraction data while EDS values are for large area EDS analysis that may include impurities.

Fe composition			a	c	T_C	μ_{sat}	μ_{eff}	T_{CW}
nominal	Rietveld	EDS	(Å)	(Å)	(K)	(μ_B/Fe)	(μ_B/Fe)	(K)
3.10	2.97(2)	3.07(2)	4.0244(1)	16.3293(5)	232	1.31	4.9(1)	225.6(2)
3.00	2.96(1)	3.06(3)	4.0184(1)	16.3344(4)	226	1.32	4.8(1)	221.7(1)
2.90	2.92(1)	2.92(3)	4.0013(1)	16.3494(4)	220	1.28	4.4(1)	218.9(1)
2.85	2.87(1)	2.88(2)	3.9840(1)	16.3676(3)	203	1.27	4.4(1)	203.2(1)
2.80	2.78(1)	2.81(2)	3.9564(1)	16.3947(4)	154	1.08	4.5(1)	143.5(3)
2.75	2.69(4)	2.79(3)	3.9475(4)	16.405(1)	140	1.04	3.9(2)	142.6(2)

for our polycrystalline samples. The RWR provides a quick means to characterize the degree to which a magnetic moment is localized. RWR is defined as RWR $= p_c/p_s$, with p_c obtained from the effective moment $p_c(p_c+2) = p_{eff}^2$.[30,31] Physically, p_c is the saturation moment expected from the effective moment calculated from the susceptibility in the paramagnetic phase (assuming Curie-Weiss behavior) and p_s is the saturation moment obtained in the ordered state. RWR = 1 for localized systems and is larger in an itinerant system, with the ratio increasing as T_C decreases for itinerant systems. Here, we take p_s as the magnetization obtained at 2 K and 60 kOe and calculate RWR values between 2.7 and 3.4 for our polycrystalline samples. These values are fairly similar to the RWR = 3.8 reported in Ref. 20.

The observation of RWR > 1 in compounds with a low Curie temperature ($T_C \lesssim 500$ K) suggests itinerant ferromagnetism is likely present. In comparison to the values tabulated by Wohlfarth in 1978 and Moriya in 1979, these $Fe_{3-x}GeTe_2$ compounds lie in the region between localized and itinerant ferromagnetism.[30,31] We do not observe a strong magnetoelastic effect at the transition, which is expected for large RWR (itinerant) systems.[30] While we do not observe a strong increase in the RWR values as T_C decreases, this can likely be attributed to the influence of vacancies on the structure and magnetism (multiple effects influencing both T_C and RWR). Future measurements of the spin-waves via inelastic neutron scattering will aid in addressing the itinerant nature of this system, as would theoretical or experimental studies into the influence of pressure on T_C.

We have summarized the magnetization data as a plot correlating the lattice parameters with the Curie temperature, shown in Fig. 10. In addition, Table IV provides a summary of sample compositions determined using various methods as well as the magnetic properties. T_C clearly decreases as Fe vacancies are introduced and the lattice responds with a decrease in the in-plane lattice parameter and a slight expansion along $\boldsymbol{c}$. These results can be used as a guide to predict the composition needed to obtain a particular T_C or as a means to expedite characterization, and must be considered when performing measurements on ultra-thin samples. Figure 10 shows that the flux-grown crystals do not behave unexpectedly based on the behavior of polycrystalline materials.

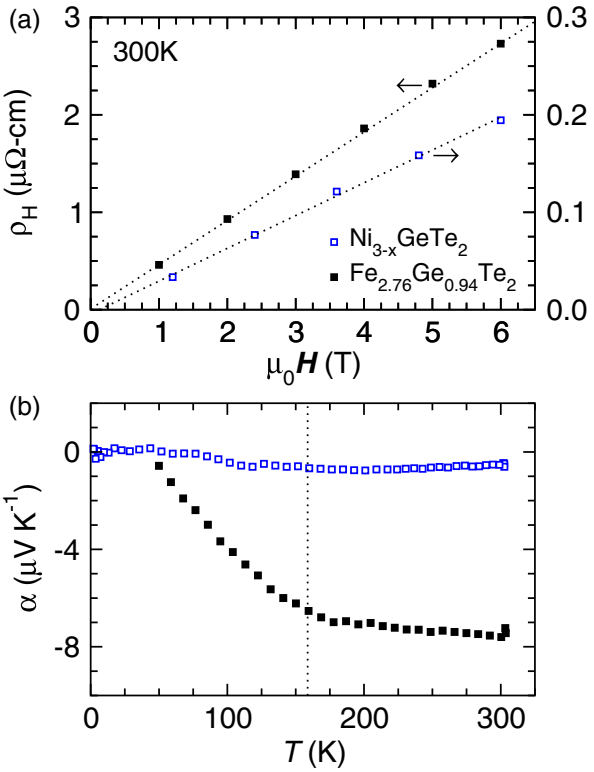

FIG. 11. (color online) (a) Hall resistance as a function of applied field suggests p-type conduction in $Fe_{2.76}Ge_{0.94}Te_2$ and $Ni_{3-x}GeTe_2$ crystals, while in (b) the negative Seebeck coefficients indicates n-type conduction. The dashed line in panel (b) indicates the Curie temperature of the $Fe_{2.76}Ge_{0.94}Te_2$ crystal.

D. Hall Effect and Seebeck Coefficients

We have utilized Hall effect and thermoelectric measurements to characterize the in-plane electrical transport in $Fe_{2.76}Ge_{0.94}Te_2$ and $Ni_{3-x}GeTe_2$ crystals. These results, summarized in Fig. 11, reveal that both systems likely have multiple carrier types contributing to conduction. We observe positive Hall coefficients and negative Seebeck coefficients, which would independently suggest p-type and n-type conduction, respectively. The linear dependence of the Hall resistance on applied field prohibits a detailed analysis aimed at determining the con-

tribution of each band/carrier-type. Theoretical calculations would provide additional insight into the origin of this apparent multi-carrier transport. We note that our flux-grown crystals of $Ni_{3-x}GeTe_2$ likely have $x \approx 0.6$ based on EDS measurements.

At room temperature, the Hall coefficient R_H of $Ni_{3-x}GeTe_2$ is about an order of magnitude smaller than that of $Fe_{2.76}Ge_{0.94}Te_2$, which translates to a larger hole concentration in $Ni_{3-x}GeTe_2$ if a single-carrier model is used. Specifically, at 300 K the Hall carrier density $n_H = 1/R_H e$ is approximately $1.8\times10^{22}cm^{-3}$ for $Ni_{3-x}GeTe_2$ and approximately $1.9\times10^{21}cm^{-3}$ for $Fe_{2.76}Ge_{0.94}Te_2$. If both holes and electrons are present, as suggested by these results, the Hall coefficients could be artificially reduced and the carrier concentrations reported would be upper-limits to the actual number of holes in the system. A more complete compensation of charge carriers may be responsible for the smaller Hall coefficient of $Ni_{3-x}GeTe_2$, though we found $Ni_{3-x}GeTe_2$ to have about an order of magnitude lower electrical resistivity (Supplemental Materials). As discussed in the Supplemental Materials, the Hall coefficient of $Fe_{2.76}Ge_{0.94}Te_2$ is strongly influenced by an anomalous Hall contribution below ≈200 K. Thermal conductivity and specific heat data for $Fe_{2.76}Ge_{0.94}Te_2$ and $Ni_{3-x}GeTe_2$ are also presented in the Supplemental Materials.[32]

IV. SUMMARY

The availability of $Fe_{3-x}GeTe_2$ and other recently-developed, cleavable ferromagnets provides a starting point for the development of magnetically-active van der Waals heterostructures. While such architectures will likely be designed to investigate specific physics or functionality, fundamental investigations will almost certainly yield unique spin structures or magnetotransport. This work has demonstrated that the itinerant ferromagnetism in $Fe_{3-x}GeTe_2$ can be tuned by controlling the Fe content. All manifestations of the magnetic interactions, from the Curie temperature to the local moment, are reduced as Fe vacancies are created and the in-plane lattice parameter decreases. By mapping the magnetic phase diagram of $Fe_{3-x}GeTe_2$, this work has provided a foundation for future studies examining the influence of dimensionality on the magnetism in these van der Waals bonded materials. While we have shown that the magnetic behavior can be controlled through total Fe content, chemical substitutions or intercalation may provide additional control over the magnetism and physical properties of this layered material. Future work in this area will need to examine the stability of ultra-thin $Fe_{3-x}GeTe_2$ as a function of Fe content. In addition, experiments under pressure and theoretical calculations will likely provide valuable information regarding the interactions between the electronic and magnetic structures of these multi-carrier, itinerant ferromagnets.

V. ACKNOWLEDGEMENTS

This work was supported by the U. S. Department of Energy, Office of Science, Basic Energy Sciences, Materials Sciences and Engineering Division. Research performed at the High Flux Isotope Reactor at Oak Ridge National Lab was supported by the Department of Energy, Scientific User Facility Program. We thank Radu Custelcean for assistance with single crystal x-ray diffraction data collection.

* mayaf@ornl.gov

[1] A. K. Geim and I. V. Grigorieva, Nature **2013**, 4191 (2013).
[2] M. Chhowalla, H. S. Shin, G. Eda, L.-J. Li, K. P. Loh, and H. Zhang, Nat. Chem. **5**, 263 (2013).
[3] G. R. Bhimanapati, Z. Lin, V. Meunier, Y. Jung, J. Cha, S. Das, D. Xiao, Y. Son, M. S. Strano, V. R. Cooper, L. Liang, S. G. Louie, E. Ringe, W. Zhou, S. S. Kim, R. R. Naik, B. G. Sumpter, H. Terrones, F. Xia, Y. Wang, J. Zhu, D. Akinwande, N. Alem, J. A. Schuller, R. E. Schaak, M. Terrones, and J. A. Robinson, ACS Nano **10.1021/acsnano.5b05556**, article asap (2015).
[4] S. Z. Butler, S. M. Hollen, L. Cao, Y. Cui, J. A. Gupta, H. R. Gutiérrez, T. F. Heinz, S. S. Hong, J. Huang, A. F. Ismach, E. Johnston-Halperin, M. Kuno, V. V. Plashnitsa, R. D. Robinson, R. S. Ruoff, S. Salahuddin, J. Shan, L. Shi, M. G. Spencer, M. Terrones, W. Windl, and J. E. Goldberger, ACS Nano **7**, 2898 (2013).
[5] M. Massicotte, P. Schmidt, F. Vialla, K. G. Schädler, A. Reserbat-Plantey, K. Watanabe, T. Taniguchi, K. J. Tielrooij, and F. H. L. Koppens, Nat. Nanotechnol. **online pub. 10.1038/nnano.2015.227** (2015).
[6] C.-Z. Chang, P. Tang, X. Feng, K. Li, X.-C. Ma, W. Duan, K. He, and Q.-K. Xue, Phys. Rev. Lett. **115**, 136801 (2015).
[7] A. G. Swartz, P. M. Odenthal, Y. Hao, R. S. Ruoff, and R. K. Kawakami, ACS Nano **6**, 10063 (2012).
[8] H. X. Yang, A. Hallal, D. Terrade, X. Waintal, S. Roche, and M. Chshiev, Phys. Rev. Lett. **110**, 046603 (2013).
[9] X. Z. Yu, N. Kanazawa, Y. Onose, K. Kimoto, W. Z. Zhang, S. Ishiwata, Y. Matsui, and Y. Tokura, Nat. Mat. **10**, 106 (2011).
[10] S. Banerjee, J. Rowland, O. Erten, and M. Randeria, Phys. Rev. X **4**, 031045 (2014).
[11] L. D. Casto, A. J. Clune, M. O. Yokosuk, J. L. Musfeldt, T. J. Williams, H. L. Zhuang, M.-W. Lin, K. Xiao, R. G. Hennig, B. C. Sales, J.-Q. Yan, and D. Mandrus, APL Materials **3**, 041515 (2015).
[12] N. Sivadas, M. W. Daniels, R. H. Swendsen, S. Okamoto, and D. Xiao, Phys. Rev. B **91**, 235425 (2015).
[13] T. J. Williams, A. A. Aczel, M. D. Lumsden, S. E. Nagler, M. B. Stone, J.-Q. Yan, and D. Mandrus, Phys. Rev. B **92**, 144404 (2015).

[14] M. A. McGuire, H. Dixit, V. R. Cooper, and B. C. Sales, Chem. Mater. **27**, 612 (2015).
[15] W.-B. Zhang, Q. Qu, P. Zhu, and C.-H. Lam, arXiv:1507.07275 (2015).
[16] V. Carteaux, F. Moussa, and M. Spiesser, Europhys. Lett. **29**, 251 (1995).
[17] M.-W. Lin, H. L. Zhuang, J. Yan, T. Z. Ward, A. A. Puretzky, C. M. Rouleau, Z. Gai, L. Liang, V. Meunier, B. G. Sumpter, P. Ganesh, P. R. C. Kent, D. B. Geohegan, D. G. Mandrus, and K. Xiao, J. Mater. Chem. C , online pub. 10.1039/c5tc03463a (2015).
[18] H.-J. Deiseroth, K. Aleksandrov, C. Reiner, L. Kienle, and R. K. Kremer, Eur. J. Inorg. Chem. **2006**, 1561 (2006).
[19] K. Kanematsu, J. Phys. Soc. Jap. **20**, 36 (1965).
[20] B. Chen, J.-H. Yang, H.-D. Wang, M. Imai, H. Ohta, C. Michioka, K. Yoshimura, and M.-H. Fang, J. Phys. Soc. Jap. **82**, 124711 (2013).
[21] V. Y. Verchenko, A. A. Tsirlin, A. V. Sobolev, I. A. Presniakov, and A. V. Shevelkov, Inorg. Mater. **54**, 8598 (2015).
[22] G. M. Sheldrick, Acta Cryst. **A64**, 112 (2008).
[23] E. Parthe and L. M. Gelato, Acta Cryst. **A40**, 169 (1984).
[24] A. L. Spek, Acta Cryst. **D65**, 148 (2009).
[25] J. Rodrguez-Carvajal, Physica B **192**, 55 (1993).
[26] B. Malaman, J. Steinmetz, and B. Roques, J. Less-Common Metals **75**, 155 (1980).
[27] H. Katsuraki, J. Phys. Soc. Jap. **19**, 863 (1964).
[28] E. Germagnoli, C. Lamborizio, S. Mora, and I. Ortalli, Il Nuovo Cimento **42B**, 314 (1966).
[29] F. Albertini, L. Pareti, A. Deriu, D. Negri, G. Calestani, O. Moze, S. J. Kennedy, and R. Sonntag, J. Appl. Phys. **84**, 401 (1998).
[30] E. P. Wohlfarth, J. Mag. Mag. Mater. **7**, 113 (1978).
[31] T. Moriya, J. Mag. Mag. Mater. **14**, 1 (1979).
[32] See Supplemental Material at [URL will be inserted by publisher] for powder neutron diffraction data, anomalous Hall effect data, electrical resistivity, thermal transport, and specific heat data.